

International Conference on Space Optics—ICSO 2006

Noordwijk, Netherlands

27–30 June 2006

Edited by Errico Armandillo, Josiane Costeraste, and Nikos Karafolas



An ultra-lightweight, large aperture, deployable telescope for advanced lidar applications

P. Mazzinghi, V. Bratina, D. Ferruzzi, L. Gambicorti, et al.



AN ULTRA-LIGHTWEIGHT, LARGE APERTURE, DEPLOYABLE TELESCOPE FOR ADVANCED LIDAR APPLICATIONS

P. Mazzinghi¹, V. Bratina¹, D. Ferruzzi¹, L. Gambicorti¹, F. Simonetti¹, A. Zuccaro Marchi¹, P. Salinari², F. Lisi²,
M. Olivier³, A. Bursi³, J. Pereira do Carmo⁴

¹National Institute of Applied Optics (INOA-CNR), Largo Enrico Fermi, 6 – 50125 Firenze, Italy
Emails: piero.mazzinghi@inoa.it, vojko.bratina@inoa.it, debora.ferruzzi@inoa.it, lisa.gambicorti@inoa.it,
francesca.simonetti@inoa.it, alessandro.zuccaro@inoa.it

²INAF, Arcetri Astrophysics Observatory, Largo Enrico Fermi, 6 – 50125 Firenze, Italy
Emails: salinari@arcetri.astro.it, lisi@arcetri.astro.it

³Carlo Gavazzi Space (CGS) via Gallarate, 15 – 20151 Milano, Italy, Emails: molivier@cgspace.it, abursi@cgspace.it

⁴Europe Space Agency ESTEC/TEC-MMO, Keplerlaan 1 – 2200 AG Noordwijk, The Netherlands
Email: Joao.Pereira.Do.Carmo@esa.int

ABSTRACT

This work presents a new technological concept for large aperture, lightweight, telescopes using thin deployable active mirrors, currently under a feasibility study for spaceborne Lidars.

The study is mainly addressed to a DIAL (Differential Absorption Lidar) at 935.5 nm for the measurement of water vapour profile in atmosphere, to be part of a typical small ESA Earth Observation satellite to be launched with ROCKOT vehicle. A detailed telescope optical design will be presented, including the results of angular and spatial resolution, effective optical aperture and radiometric transmission, optical alignment tolerances, stray-light and baffling. Also the results of a complete thermo-mechanical model will be shown, discussing temporal and thermal stability, deployment technology and performances, overall mass budget, technological and operational risk and system complexity.

Keywords: deployable telescope, space lidar, active optics, large aperture telescope, optical design and stray-light.

1. INTRODUCTION

This study activity responds to ESA's "Advanced LIDAR Concepts" proposal for the development of advanced Light Detection & Ranging (LIDAR) technologies, in particular for the use of large aperture telescope to retrieve a sufficient signal with a moderate power laser transmitter. The first part of the paper describes the study development, starting from the requirements analysis up to the selection of the best solution or base line amongst various candidates. To achieve the requirements for a 7 m² collecting aperture telescope, with less than $\lambda/3$ wavefront error when operative after launch and deployment, a thin deployable mirror active primary telescope has proven to be the most suitable solution after an extensive trade-off. The proposed structure is a segmented

primary mirror, composed of a very rigid carbon-fiber composite back-plane and a thin Zerodur glass shell supported by a set of high efficiency electromagnetic, actively controlled actuators. Since the overall results show near diffraction-limited performances, the proposed technology has also the potential to be extended even further from the specifications of the present project, such as for high performance imaging from a large telescope for astronomic applications.

2. SPACE LIDAR TELESCOPE DESIGN

The preliminary study considered three possible solutions for a space lidar telescope, taking into account the mission requirements, listed in Tab. 1.

Tab. 1. Requirements for the Water Vapour mission.

Requirement	Value
Wavelength	935.5 nm
Field of View (FOV)	115 μ rad
Beam diameter at filter stage	< 100 mm
Acceptance angle at filter stage	± 6 mrad
Collecting efficiency	>95%
Transmission up to filter stage	>80%
Effective aperture area	> 7 m ²

The first solution is a multi pupil system, with a set of seven small on-axis afocal telescopes. This idea was early discarded because of its high costs, volume and mass, besides the difficulty in keeping the relative alignment. The second concept is based on a single pupil off-axis afocal telescope, but it is critical for tolerances and the filter specifications are not completely fulfilled. The last configuration is a single pupil on-axis afocal system, consisting of an on-axis afocal telescope with auxiliary optics. This solution is the baseline configuration, satisfying the requirements in Tab.1 with advantages of reduced volume and costs.

2.1 Baseline solution

The optical design consists of a double afocal telescope (two mirrors-four reflections), followed by a beam splitter that divides the beam in two parts, one going to the filter stage, while the other is focused by a spherical lens to the wavefront sensor stage. The components are: two parabolic mirrors (first afocal telescope), where the beam impinges twice per mirror, a beam splitter, a spherical lens and three folding mirrors as shown in Fig. 1.

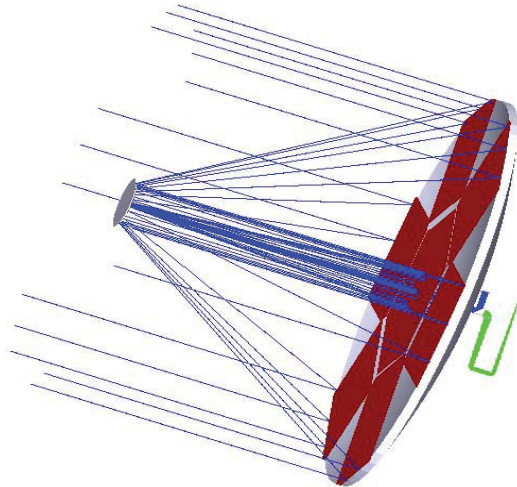


Fig. 1. Baseline optical configuration

Distance between primary and secondary mirrors is 3.15 m, maximum aperture is 4 m and the auxiliary optics size fits the rear box dimension (yellow box in Fig. 6).

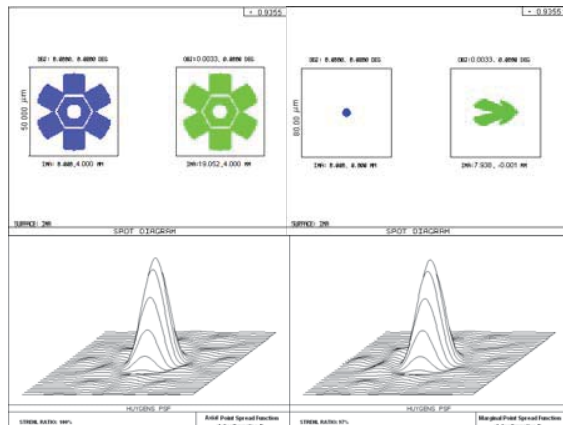


Fig.2 Spot diagrams on filter stage (left), on wavefront sensor (right) and PSF (Point Spread Function) (below) both on axis and on maximum field (0.0033 deg).

The configuration was analytically studied at first order and optimised at the third order before the final optimisation and ray tracing simulation of performances, which was done with ZEMAX® EE software.

The image quality on the wavefront sensor stage is diffraction-limited all over the FOV, with 80 μm Airy disks diameter. Strehl ratios are 100% on-axis and 97% at maximum FOV [1]. Also the quality image on filter stage satisfies the requirements (Fig. 2).

3. TOLERANCE ANALYSIS RESULTS

3.1 Tolerance budget

The sensitivity analysis has evidenced that the secondary mirror is the most sensitive element; consequently, the secondary mirror determines the error budget [2]. The results are summarized in Tab. 2, which describes the maximum errors that a parameter (radius, thickness) of an optical element must have to satisfy the requirement on wavefront sensor, which is the most critical.

Tab. 2. Tolerance budget for baseline configuration.

TOLERANCE BUDGET						
Surface	Radius (mm)	TOL	Thickness (mm)	TOL	Decen-ter (mm)	Tilts x-y
Primary mirror	6400	-0.018 +0.024	2865	-0.01 +0.01	-	-
Secon-dary mirror	670	-0.024 +0.018	3100	-	±0.008	±0.001
Lens	684	±10	3	±10	±5	X→1° Y→2°
Lens	-	-	-	-	-	-

3.2 Wavefront error estimate

Propagation of wavefront error shows that to obtain a λ/3 wavefront error ε_w on the filter stage, the surface error σ on primary mirror must be σ_M=λ/8 for baseline configuration. This value is difficult to obtain for a large area space mirror, thus evidencing the necessity of an active feedback control of this surface (§ 5.2).

4. STRAY-LIGHT AND BAFFLING

Baffling an optical system is required to reduce the propagation and detection of undesired flux, generally named “Stray-light” [3]. The term “out-of-field stray-light” indicates the light scattered by optical surfaces, by mechanical structures and interactions between them, when the light source is seen at various off-axis angles. The baffles modelling has been made with ZEMAX® EE optical software using a non sequential ray tracing to allow: a) analysis of the scattering from all surfaces behind and forward the defined light direction; b) insertion of coating on surfaces taking into account the scattering also from non optical surfaces as baffles, spiders and other mechanical

structures [4]. A first order correction of the stray-light was performed to design the baffles on M1 and M2 to minimize the direct light that reaches the detector without interacting with the mirrors (Fig. 3) [5]. The non-sequential analysis of the optical system has been implemented with the study of the double reflections due to the direct and indirect scattering on the optical surfaces and on the baffles on M1 and M2. All double reflections have been evaluated with a scanning step of 0.05 deg. The most critical double reflection is between M1 and M4 (in a narrow range of angles around 0.3 deg). To eliminate this contribution, a third conic internal baffle has been inserted on M3.

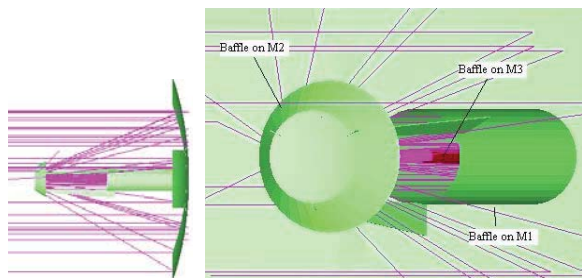


Fig. 3. Telescope with baffles on M2 and M1 (left), baffles on M1, M2 and M3 (right).

4.1 Point source transmittance of the instrument

The Point Source Transmittance (PST) curve of the instruments quantifies the radiometric transmission in the FOV and evaluates out-of-field stray-light. The parameters for the analysis are summarized in Tab. 3.

Tab. 3. Parameters of the double reflection order stray-light analysis.

Source	Flat, Lambertian
Total power	1 Watt
Number of rays	2 10 ⁶
Minimum relative ray intensity	10 ⁻¹³
Coatings on M1 and M2	GOLD R=98% at 935±50 nm
Electrochemical treatment on back shade, spiders, baffles	CHEMGLAZED Z302 R= 2% at 935±50 nm

The PST of the telescope is reconstructed moving a flat source at several off-axis angles and reporting the value on the detector normalised to the primary effective area [6]. When the off-axis angle is in the optimised FOV of the telescope (i.e.± 0.00324 deg) we have an information on the efficiency of the optical system referred to the effective area of the primary mirror. In the range between 0.003 deg up to about 0.012 deg the light normally reflected by the optical system decreases and from 0.012 deg up to 69 deg the light reaching the detector is only the scattered component.

The scattered light comes from gold-coated mirrors, from the spiders and from back shade behind the primary mirror.

When the three baffles on M1, M2 and M3 are inserted, the central obstruction increases and the efficiency in the FOV decreases from 86.6% to 73.7% but at the same time the level of scattered light in the out-of-field range changes from a mean value of 10⁻⁴ up to 10⁻⁸.

This large decrement in the stray-light is important to increase the signal-to-noise ration, which improves the LIDAR detection and permits a good wavefront sensing. Fig. 4 shows the PST of the system with/without baffles.

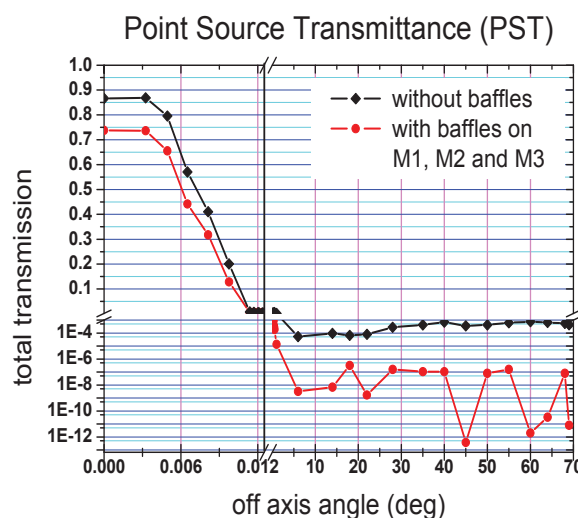


Fig. 4. The PST with/without baffles.

4.2 Integral of the stray-light from Earth

The total stray-light coming from the in-field and out-of-field irradiance due to the back scattering from Earth atmosphere is the integral of the transmission resulting from the model for field angles from 0 deg up to about 69 deg [7] [8].

Tab. 4. Parameters for the numerical integration.

Scattering from Earth	Lambertian
Detector distance	450 km
Ray of the Earth	6360 km
Half illuminated earth	
Albedo	0.3
Incidence angle of the solar light on the Earth	85 deg
Value at 935 nm [9]	1.1 (Watt/ m ² /nm)

A numerical integral of this contribute has been evaluated considering the parameters in Tab. 4 and the results after the integration are in Tab.5.

Tab. 5 Results for the cumulative irradiance.

OFF AXIS ANGLE (DEG)	CUMULATIVE IRRADIANCE (WATT/M ² /NM)
0÷0.0120 (In field)	1.23E-01
0.0120÷69 (Out of field)	1.70E-03

Therefore, the main result is that the contribution due to the out-of-field stray-light is about 1.38 % with respect to the in-field background, so the off-field stray-light is negligible with respect to the signal background.

5. MECHANICAL STRUCTURE AND ACTIVE SURFACE CONTROL

The proposed mechanical design for the LIDAR telescope is based on a typical Cassegrain architecture with deployable primary mirror and fixed secondary. The key features of the design, and current goal for the preliminary design, are:

- Large optics (total available primary mirror surface about 10 m²);
- Lightweight design (primary mirror areal density about 15 Kg/m²);
- High wave front quality ($< \lambda/3$).

The deployable mirror technology under study allows obtaining a large area for observation using a compact stowing volume, compatible with ROCKOT class launchers [10]. Fig. 5 shows the stowed and Fig. 6 deployed configuration, highlighting some satellite subsystems and the launcher overall dimensions. It can be seen that the overall architecture is a standard for this kind of telescopes, based on high stability CFRP (Carbon Fiber Reinforced Plastic) structures deployed with precision hinge systems.

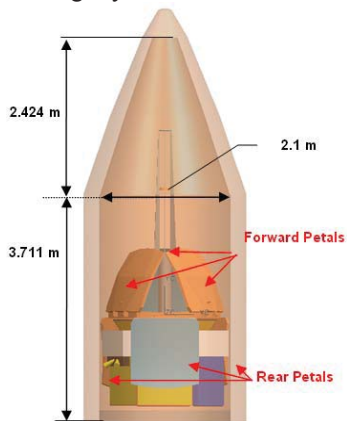


Fig. 5. LIDAR Satellite stowed.

For the current baseline of the satellite design, the forward and rear petals deployment kinematics has been selected, in order to guarantee the best compromise between the deployed surface and the deployment simplicity.

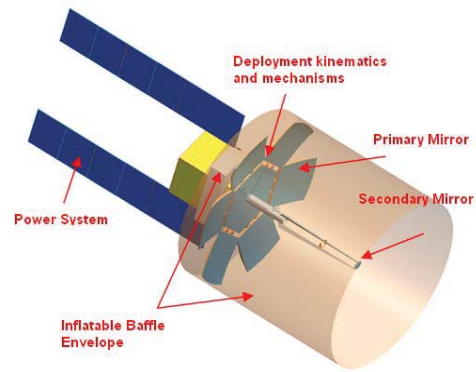


Fig. 6. LIDAR Satellite deployed configuration.

The current trade-off between preloaded linear revolute joints, tape-spring rolling hinges, active deployment mechanisms, indicate also that Elastic Memory Composite (EMC) actuators [11] can be a suitable actuator associated to a rod kinematics (Fig. 7-8), to obtain a highly precise deployment (the error can be simply recovered by the actuator) with the required reliability.

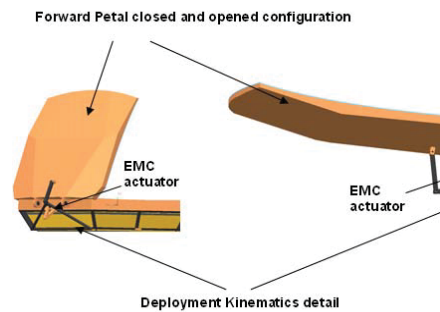


Fig. 7. Deployment rod kinematics for the forward petals.

The presented concept can be scaled up using more complex mechanical deployment schemes, that, once proven the capability of the locking and actuation system of the thin mirror, could lead to very large and lightweight space optics with a substantial cost reduction for their manufacturing integration and testing.



Fig. 8. EMC actuator example in the stowed and deployed configuration.

5.1 Electrostatic locking

The innovative approach for the primary mirror is based to the coupling of a thin Zerodur mirror optical surface 1 mm thick with a lightweight CFRP back-

plane and supporting structure. A major problem is how to preserve the integrity of the glass shell in the harsh environment of the launch. We propose to use electrostatic force for attracting the glass (suitably coated with a conductive coating on its back face) toward the back plane, in turn coated with a conductive layer and an insulating layer of high dielectric constant (Mylar) interposed. This method is particularly promising due to the low power consumption and to the low "extra material" budget it requires. For an average insulation thickness of $10\ \mu\text{m}$, $\epsilon = 4$ and $100\ \text{V}$ potential difference, the attractive force is $\sim 7000\ \text{N/m}^2$, while the mirror mass is $\sim 2.5\ \text{kg/m}^2$. The mirror would detach (axially) from the back plate only with an acceleration of $\sim 285\ \text{g}$. For a reasonably high friction coefficient (>0.3) also the lateral motion would be prevented for accelerations of $\sim 100\ \text{g}$. As the "gluing" force depends critically on the thickness (and on possible gaps between glass and back plate) in the electrostatic "sandwich", it is needed to assure that the insulating layer is of constant thickness and in contact with the (conducting) back surface of the thin mirror. The necessary good matching between glass and back plate could be obtained with a replication technique that will be studied and demonstrated experimentally.

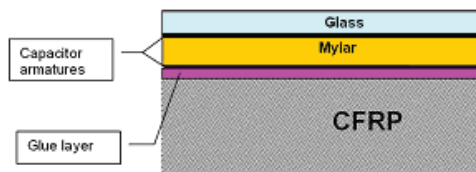


Fig. 9. Scheme of Electrostatic Locking.

Fig. 9 shows the Electrostatic Locking conceptual layout that can be able to assure the mirror survivability at launch. Then the mirror is activated by a set of electromagnetic actuators that shall control its shape to the desired shape accuracy.

5.2 Active control analysis

After release of the thin mirror from the back plane a set of actuators shall recover the shape error using an active control system able to guarantee $< \lambda/3$ wave front quality using very low power. The main structural deformations are caused by deployment error; mirror manufacturing error and thermal deformation.

The active control of the segmented primary mirror relies on the interaction between several independent systems that concur to implement a closed control loop: a) the reference signal that comes from the retro-scattered light of two laser diodes mounted on the satellite, focused on the ground by the Lidar telescope and collected by the optical system to be controlled, b) the wavefront sensing system that measures the aberration of the collected wavefront, c) the computer where a control algorithm takes care of translating the

measured optical data into electrical signals that drive the actuators, and d) the mechanical actuators that apply forces to deform the mirror. The designed actuators are able to recover all these errors guaranteeing the required optical performance with really low power consumption (fraction of Watt per actuator). The current electromagnetic actuator design is showed in Fig. 10. The actuator design depends on a long experience of active secondary mirrors on ground-based telescopes [12]. To the purposes of the present application, it has been developed according to the following guidelines.

1. **Size and mass.** The actuators pitch (spacing) on each petal was consolidated by preliminary optical and dynamics analysis. It resulted that such spacing would not be smaller than hundreds mm, 250 mm in the present layout. The actuator diameter is set to about $25\div 30\text{mm}$. This is going to allow easier and safer prototyping and testing of the actuator, in particular for what concerns the position (capacitive) sensor implementation. Actuator overall length will be tuned to maximize both electromagnetic efficiency and sensor resolution, with the constraint of the mass budget for each petal.

2. **Guiding.** The actuator concept presented relies on a precise guiding of the mobile equipment (holding the magnets) with respect to the fixed frame (coil bobbins). The baseline idea is to use a pair of axial bearings to guide the two parts. The drawback of such approach is the possible non-linear effects introduced into the position control by bearings stick-slip. Preliminary measurements confirm this is not a problem if the control loop has sufficient bandwidth.

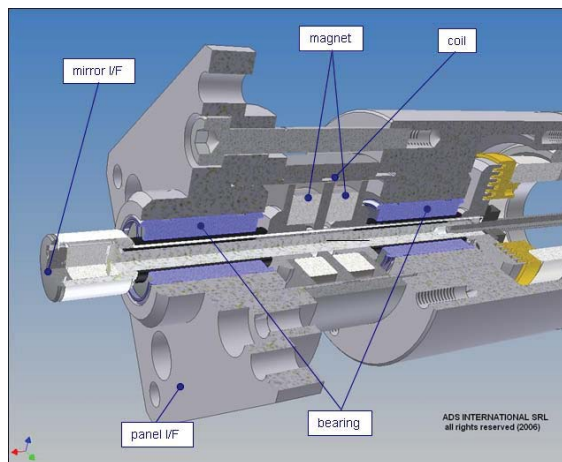


Fig. 10. Active mirror control Actuator.

3. **Thermal efficiency.** Actuator current design is consistent with an overall power dissipation of the order of $200\ \text{mW/act}$. This figure includes the contribution of about $50\ \text{mW}$ dissipated at coil level and $150\ \text{mW}$ on the electronics. The latter is generated by the contribution of capacitive sensor conditioning electronics, digital control

electronics and actuator power driver. Electromagnetic efficiency is expected to be of the order of $1/\sqrt{W}$ which will provide up to 200 mN force per actuator on the mirror.

6 ALIGNMENT AND STABILITY

A critical point concerns the strategy to align each segment of the mirror with the others, having in mind the limited capability of wavefront sensors when we call for correction of piston-induced aberrations. This problem is more critical just after deployment because the relative positioning of each segment relies only on the accuracy of the hinges, which cannot be as good as requested by the range of correction of piston aberration.

We propose to use a composed metrology system that recovers the accuracy needed to reach the range where the control loop can take charge of the aberration control. Each actuator has its own metrology (based on capacitive sensors with a sensitivity of the order of a few nanometers), giving the relative position of the mirror patch and the backplane with high accuracy. The facing sides of the backplanes have capacitive sensors that can be calibrated up to a few micrometers. After the deployment, we take the central segment of the mirror as starting point to align all the other segments; the first step is to measure the linear and the angular displacement relative to the two segments and to use these information to move the actuators up to get an alignment between the mirror segments that is less than 15-20 μm . The procedure is extended to the full set of segments, and can be repeated if necessary. To reach the needed accuracy, we propose to exploit the retro-scattered optical signal coming from two light beams at two slightly different wavelengths (λ_1 and λ_2) as a probe for the sensing system to reach the control range of the wavefront sensor. The wavefront sensor has an output that is a sinusoid when we shift the piston error between two segments of one wavelength. When the output is exactly a null at λ_1 , the piston error is a multiple of that wavelength; at this point, if we fire the second laser that has a slightly different wavelength λ_2 , we can easily detect the sign of the piston error from the wavefront sensor. After commanding a translation of one wavelength, we can fire again the λ_1 laser to repeat the search of null position, the λ_2 laser to find the error sign, and so on up to the convergence of the process, when the wavefront corrector is inside its capture range.

7 CONCLUSION

The technology proposed in this work is a step forward in the possibility to develop large area telescopes to be deployed in orbit. The decoupling of the mirror optical surface from the supporting mechanics improves the optical precision and reduces the requirements for the tolerances in the mechanics itself and in the deployment mechanism. All this leads in reduction of weight both of the optical surface

and the mechanics, permitting much larger telescopes to be developed. In the present application for Earth observation, the surface control feedback uses a low power dedicated laser. This can be achieved by any point source in the FOV (a potential further step for this technology) for astronomical applications such as the study of high-energy cosmic rays from space [13].

8 ACKNOWLEDGMENTS

The authors are grateful to the Europe Space Agency (ESA) for the opportunity offered to develop this research under the contract AO/1-4629/NL/CP.

The authors are grateful to the ADS International SRL for picture on the actuator.

9 REFERENCES

1. Wetherell W. B., "The calculation of image quality", Applied Optics and Optical Engineering, Shannon and Wyant, Vol. VIII, cap. 6 appendix B, Pergamon Handbook, 1980.
2. Ginsberg R. H., *Outline of tolerancing (from performance specification to tolerance drawings)*, Optical Engineering, Vol.20 (2), 175-180, March/April 1981.
3. Wyatt C. L., "Radiometric system design", Cap 14, Macmillan Publishing Company, New York 1987.
4. Breault R. P. and Milsom D., Breault Research Organization, Tucson Arizona, "Stray Light analysis of the Cassini Telescope", SPIE vol. 1753/210-227 Stray radiation in Optical System II, 1992.
5. Arnoux J. J., Matra Marconi Space France department of Optical Engineering, "Star sensor baffle optimization: same helpful practical design rules", SPIE vol. 2864/333-338, 1996.
6. Illumination and Stray-Light Analysis using ZEMAX, manuals of Zemax package.
7. Grum and Bartleson, "Optical Radiation Measurements", Vol 2, Academic Press, New York 1980.
8. Fazio., "Dizionario e manuale delle unità di misura III", SI, MKSA, CGS & Co, Zanichelli, Bologna 1985.
9. Wehrli85_airmas0_irradiances:
<http://redc.nrel.gov/solar/spectra/am0/wehrli1985.new.html>
10. "ROCKOT Launcher User Guide Issue 4" Eurockot Launch Service Provider.
11. Francio W. et al, "Development of an EMC Self-Locking Linear Actuator for Deployable Optics"; 45th AIAA/ASME/ASCE/AHS/ASC Structures, Structural Dynamics, and Materials Conference, Palm Springs, CA, April 2004.
12. Del Vecchio C. et al, "Selecting the electromagnetic actuator of the ELT primary mirror", SPIE Proceedings on Astronomical Telescopes and Instrumentation, Orlando (USA), 24-31 May 2006.
13. Mazinghi P. et al, "Large aperture and wide field of view space telescope for the detection of ultra high energy cosmic rays and neutrinos", this Conference Proceedings.